Enhanced electrochemical performances and thermal stability of $LiNi_{1/3}Co_{1/3}Mn_{1/3}O_2$ by surface modification with YF_3

Longchuan Chen, Yanmin Yang, Zhisheng Wang, Zhiya Lin, Jingying Zhang, Qiuling Su, Yue Chen, Wei Chen, Yingbin Lin, Zhigao Huang

PII: S0925-8388(17)30909-X

DOI: 10.1016/j.jallcom.2017.03.130

Reference: JALCOM 41168

To appear in: *Journal of Alloys and Compounds*

Received Date: 21 November 2016

Revised Date: 7 March 2017

Accepted Date: 12 March 2017

Please cite this article as: L. Chen, Y. Yang, Z. Wang, Z. Lin, J. Zhang, Q. Su, Y. Chen, W. Chen, Y. Lin, Z. Huang, Enhanced electrochemical performances and thermal stability of $LiNi_{1/3}Co_{1/3}Mn_{1/3}O_2$ by surface modification with YF_3, *Journal of Alloys and Compounds* (2017), doi: 10.1016/j.jallcom.2017.03.130.

Enhanced electrochemical performances and thermal stability of $LiNi_{1/3}Co_{1/3}Mn_{1/3}O_2$ by surface modification with YF_3

Longchuan Chen[1], Yanmin Yang[1], Zhisheng Wang[1], Zhiya Lin[1], Jingying Zhang[1], Qiuling Su[1], Yue Chen[1], Wei Chen[1], Yingbin Lin[1,2]*, Zhigao Huang[1,2]

1. College of Physics and Energy, Fujian Normal University, Fujian Provincial Key Laboratory of Quantum Manipulation and New Energy Materials, Fuzhou，350117, China.
2. Fujian Provincial Collaborative Innovation Center for Optoelectronic Semiconductors and Efficient Devices, Xiamen, 361005, China

*Corresponding author: Yingbin Lin

Tel: +86-591-2286-8132

Fax: +86-591-2286-8132

E-mail: yblin@fjnu.edu.cn

Abstract

Layered $LiNi_{1/3}Co_{1/3}Mn_{1/3}O_2$ cathode materials were prepared using a sol-gel method and subsequently surface-modified with YF_3 layer by a wet chemical process. In comparison with pristine $LiNi_{1/3}Co_{1/3}Mn_{1/3}O_2$, $LiNi_{1/3}Co_{1/3}Mn_{1/3}O_2@YF_3$ exhibited higher rate capability, better cyclability and better thermal stability. After 100 cycles at 5 C and 25°C, $LiNi_{1/3}Co_{1/3}Mn_{1/3}O_2@YF_3$ showed 93% capacity retention compared with 74% for pristine $LiNi_{1/3}Co_{1/3}Mn_{1/3}O_2$. Electrochemical measurements demonstrated that the improved electrochemical performances of YF_3-coated $LiNi_{1/3}Co_{1/3}Mn_{1/3}O_2$ might be attributed to smaller charge-transfer resistance, higher lithium diffusion rate, more stable electrolyte/electrode interfacial structure, and lower activation energy. Kelvin probe force microscopy measurements revealed that the $LiNi_{1/3}Co_{1/3}Mn_{1/3}O_2@YF_3$ cathode possessed a lower surface potential and work function than those of the pristine one, which help to facilitate electron transport and suppress reactions between the electrolyte and cathode during the charge/discharge processes. In a certain way, the reported results clarified the possible mechanism of the enhanced performances of cathode materials with surface modification in terms of interfacial effect.

Keywords**:** Lithium-ion batteries; Lithium nickel cobalt manganese oxide; Surface modification; Diffusion coefficient; Kelvin probe force microscopy.

1. Introduction

In recent years, high energy density cathode materials for lithium-ion secondary batteries have garnered increased interest due to their potential application in electric vehicles (EVs), hybrid electric vehicles (HEVs) and plug-in hybrid vehicles (PHEV) [1-5]. Among the prospective cathode materials, hexagonal α-$NaFeO_2$-type $LiNi_{1/3}Co_{1/3}Mn_{1/3}O_2$ has attracted increasing attention due to its high discharge capacity, excellent structural/thermal stability and low cost [6,7]. However, $LiNi_{1/3}Co_{1/3}Mn_{1/3}O_2$ cathodes also suffer from poor rate performance, cycling stability and thermal safety, resulting from phase transitions and severe side reactions between electrolyte species and hydrofluoric acid (HF) [8,9]. To circumvent the significant drawbacks, tremendous efforts have been implemented such as the fabrication of nanosized $LiNi_{1/3}Co_{1/3}Mn_{1/3}O_2$, doping with foreign atoms and surface modification. Surface modification had been proven to be an effective way in improving electrochemical performances of $LiNi_{1/3}Co_{1/3}Mn_{1/3}O_2$ cathodes [10-13]. For instance, Xie et al. [11] reported that 1wt% CeF_3-coated $LiNi_{1/3}Co_{1/3}Mn_{1/3}O_2$ could deliver a discharge capacity of 107 $mAhg^{-1}$ at 5C rate. Zhang et al. [13] reported that surface modification of $LiNi_{1/3}Co_{1/3}Mn_{1/3}O_2$ with fluoroborate glass resulted in stable cyclability with capacity retention of 96.8% after 50 cycles while the capacity retention of bare one is 81.4%. Although many improved electrochemical performances of $LiNi_{1/3}Co_{1/3}Mn_{1/3}O_2$ with surface modification had been reported, the enhanced mechanisms behind had been a matter of debate and disagreement. In this work, YF_3 with a wide band gap (>10eV), was selected as coating material for $LiNi_{1/3}Co_{1/3}Mn_{1/3}O_2$ cathodes because of its excellent structural stability in the HF-containing electrolyte, superior thermal stability and high ionic conductivity [14,15]. The effect of YF_3–coating on the physical properties and the electrochemical

performances of $LiNi_{1/3}Co_{1/3}Mn_{1/3}O_2$ cathodes was systematically investigated. The possible mechanism of the enhanced performances was discussed for cathode materials with surface modification in terms of interfacial effect.

2. Experimental

2.1 Preparation and characterization of cathode materials

$LiNi_{1/3}Co_{1/3}Mn_{1/3}O_2$ cathode materials were synthesized by a wet chemical method using tartaric acid as a chelating agent. In a typical synthesis, stoichiometric amounts of $CH_3COOLi•2H_2O$(Alfa Aesar), $Ni(CH_3OO)_2•4H_2O$ (Alfa Aesar), $Co(CH_3COO)_2•4H_2O$(Alfa Aesar) and $Mn(CH_3COO)_2•6H_2O$(Alfa Aesar) were thoroughly dissolved in de-ionized water containing appropriate amount of tartaric acid, followed by stirring at 90 ^oC until a polymerized gel was formed. The tartaric acid to total metal ion ratio was 2:1. The resultant precursor was calcinated at 500^oC for 5 h and subsequently calcinated at 900°C for 12 h in air to obtain a homogeneous $LiNi_{1/3}Co_{1/3}Mn_{1/3}O_2$ powder. To synthesize $LiNi_{1/3}Co_{1/3}Mn_{1/3}O_2@YF_3$, the as-prepared $LiNi_{1/3}Co_{1/3}Mn_{1/3}O_2$ cathode powders were dispersed in a $Y(NO_3)_3•9H_2O$ aqueous solution under vigorous stirring. Then, a 1M NH_4F solution was added dropwise, with the molar ratio of Y to F maintained at 1:3 and YF_3 at 2 wt.% of the $LiNi_{1/3}Co_{1/3}Mn_{1/3}O_2$ cathode material. The mixing solution was continuously stirred at 100°C until the solvent had completely evaporated. The obtained samples were sintered at 400°C for 5 h in air to obtain the YF_3–coated $LiNi_{1/3}Co_{1/3}Mn_{1/3}O_2$ product. A schematic illustration of the synthesis is shown in Fig. 1. For comparison, the pure YF_3 powders are prepared under the same preparation condition.

The structure of the as-prepared samples was characterized by X-ray diffraction (XRD, Rigaku MiniFlex II) using CuK_α radiation (λ=0.15405 nm). The morphologies, particle size and elemental composition of the as-synthesized powders were

determined by field emission scanning electron microscopy (FESEM, SU8010, Japan) equipped with an energy-dispersive spectroscopy (EDS). The microstructures in more detail were also examined with transmission electron microscopy (Tecnai G2 F20 S-TWIN). The YF_3 content in the composite was determined by inductively coupled plasma OES spectrometer (ICP). The surface potential of the cathode electrodes was characterized by Kelvin probe atomic force microscopy (KPAFM) (Bruker dimension ICON, Germany), which measured the strength of the electrostatic forces between a conductive probe and the sample.

2.2 Cell fabrication and characterization

The electrochemical performances of the as-prepared composites were evaluated with CR2025-type coin cell. The cathode slurry was prepared by mixing 80 wt.% active material ($LiNi_{1/3}Co_{1/3}Mn_{1/3}O_2$ or $LiNi_{1/3}Co_{1/3}Mn_{1/3}O_2@YF_3$) with 10 wt.% polyvinylidene fluoride (PVDF) and 10 wt.% super-P in a solvent (N-methy1-2-pyrrolidone). The slurry was then cast onto an aluminum current collector and dried under vacuum at 120 ^oC for 12 h. Coin cells were assembled in an argon-filled glove box with O_2 and H_2O content below 1 ppm, using lithium foil as anode and counter electrode, Cellgard 2300 microporous polyethylene membrane as separator, and 1 M $LiPF_6$ in a mixture of dimethyl carbonate (DMC) and ethyl carbonate (EC) (1:1 in volume) as the electrolyte. The galvanstatic charge/discharge measurements of the cells were carried out in the voltage range of 3.0-4.5V on a multichanmel battery testing system (Land CT2001A, Wuhan, China). Cyclic voltammetry (CV) measurements were performed using an Arbin instruments BT-2000 battery testing station, and the electrochemical impedance spectra of the samples were obtained by an electrochemical workstation (Zahner-Zennium) in the frequency range of 10 mHz to 100 KHz with an amplitude of 5 mV. Thermal stability

of the electrodes was examined by differential scanning calorimetry (DSC) on a TG-DSC simultaneous thermal analyzer (Netzsch STA449F3) across a temperature range of 30-400°C at a heating rate of 2°C min^{-1}. Prior to DSC measurements, the cells were charged to 4.5 V at a current of 0.1 C and then charged at 4.5 V for an additional 6 h. Then, the cells were disassembled in an argon-filled glove box and the cathode materials (containing acetylene black and PVDF) were scraped from the Al current collector. The obtained cathode materials were sealed in a stainless-steel pan for DSC measurements.

3 Results and discussion

3.1 material characterization

Fig.2 showed the XRD patterns of the pristine $LiNi_{1/3}Co_{1/3}Mn_{1/3}O_2$ and YF_3-coated $LiNi_{1/3}Co_{1/3}Mn_{1/3}O_2$ powders. All of the diffraction peaks were characteristic of a layered oxide structure based on a hexagonal α-$NaFeO_2$ structure with space group R-3m. Distinct splitting between the adjacent peaks of (108)/(110) and (006)/(102) indicated a highly ordered layered structure. Besides the main $LiNi_{1/3}Co_{1/3}Mn_{1/3}O_2$ phase, additional diffraction peaks were also observed at 27.88°, which corresponds to the (100) reflection of the hexagonal wurtzite structure of YF_3 (JCPDS No. 70-1935). In addition, there was no discernible shift in peaks or third phase, suggesting no chemical reaction occurred between the two components during the calcination process [16].

SEM images of the pristine and YF_3-coated $LiNi_{1/3}Co_{1/3}Mn_{1/3}O_2$ particles were presented in Fig. 3. As shown in Fig. 3(a,b), the pristine $LiNi_{1/3}Co_{1/3}Mn_{1/3}O_2$ particles were distributed with a particle size ranging from 200 to 300 nm and displayed a smooth surface and clear boundary, while the surface of $LiNi_{1/3}Co_{1/3}Mn_{1/3}O_2$@$YF_3$ was distinctly covered by "YF_3 moss" (Fig. 3(d)). The distribution of corresponding

elements on the cathode surface was further examined by EDS. The EDS analysis of $LiNi_{1/3}Co_{1/3}Mn_{1/3}O_2$ (Fig. 4(g)) revealed the presence of Mn, Co, Ni and O in an atomic ratio (12.31:11.04:12.33:64.32) close to the chemical formula. Element mapping of $LiNi_{1/3}Co_{1/3}Mn_{1/3}O_2@YF_3$ particles (Fig. 4) revealed that Y and F displayed the same shape as the cathode material particles, indicating that YF_3 was homogeneously distributed on the surface of $LiNi_{1/3}Co_{1/3}Mn_{1/3}O_2$ particles. The corresponding EDS result in Fig. 4(h) showed the atomic ratio of Y:Mn:Co:Ni was 0.39:8.64:9.02:9.25, which is consistent with the designed content of 2 wt% YF_3 coated in the composite. The YF_3 content in the composite was also determined to be ca. 2.12wt% by inductively coupled plasma OES spectrometer (ICP). TEM image and corresponding EDS of $LiNi_{1/3}Co_{1/3}Mn_{1/3}O_2@YF_3$ particles in Fig.5 confirmed the presence of YF_3 thin film on the surface of $LiNi_{1/3}Co_{1/3}Mn_{1/3}O_2$ particles even the content of YF_3 was low. In addition, distinct parallel fringes with a basal spacing value of approximately 0.21 nm were observed, corresponding to the (104) crystalline plane of the R3m-layered structure and indicating the high crystallinity of $LiNi_{1/3}Co_{1/3}Mn_{1/3}O_2$ phase.

The discharge capacity vs. cycle number of the pristine and $LiNi_{1/3}Co_{1/3}Mn_{1/3}O_2@YF_3$ at 0.2 C, 0.5 C, 1.0 C, 2.0 C, 3.0 C, 5.0 C, and 10 C (1C=200 $mAhg^{-1}$) between 3.0 and 4.5 V at 25°C were shown in Fig. 6(a). The cells were charged and discharged at the same current density. In comparison, the $LiNi_{1/3}Co_{1/3}Mn_{1/3}O_2@YF_3$ sample demonstrated better rate performance, especially at a higher rate. At 10C, the capacity of the $LiNi_{1/3}Co_{1/3}Mn_{1/3}O_2@YF_3$ electrode was determined to be ca. 67% (96 mAh g^{-1}) at the capacity of 143 mAh g^{-1} at 0.2 C, whereas the capacity of the pristine electrode was only 51% at the same current. The improved rate capability of $LiNi_{1/3}Co_{1/3}Mn_{1/3}O_2@YF_3$ indicated that the YF_3 coating

layer not only reduced the polarization but also increased the active material's stability at high discharge current densities. The polarization at different current densities of the pristine and YF_3-coated $LiNi_{1/3}Co_{1/3}Mn_{1/3}O_2$ was shown in Fig. 6(b,c). The discharge capacity and voltage were found to decay with increasing current density, with the pristine electrodes exhibiting a sharper decay than that of YF_3-coated material. These results might be attributed to the structural stability of the layered host crystal and the superior kinetic properties of the YF_3 coating, which mitigated the cyclic degradation of the layered oxides at high rates [17]. In addition, the YF_3-coating layer would be expected to prevent attack of the cathode by HF and suppress the increase in interfacial polarization and therefore improved the cyclic stability [18].

To understand the electron-transfer kinetics of $LiNi_{1/3}Co_{1/3}Mn_{1/3}O_2$ and $LiNi_{1/3}Co_{1/3}Mn_{1/3}O_2@YF_3$ electrodes, electrochemical impedance spectroscopy had been performed. Fig. 7(a) showed the EIS plots measured using the coin cells after the rate performance. The EIS plots for both pristine $LiNi_{1/3}Co_{1/3}Mn_{1/3}O_2$ and $LiNi_{1/3}Co_{1/3}Mn_{1/3}O_2@YF_3$ consisted of two depressed semicircles in the high-to-medium frequency range and a straight line in the low-frequency region. Such a pattern of EIS could be explained by the equivalent circuit displayed in Fig. 7(b), where the symbols, R_e, R_{sf}, R_{ct}, and R_w represent the solution resistance, the impedance of a solid-electrolyte interface (SEI) layer, the charge transfer resistance, and Warburg impedance related to the solid-state diffusion of Li^+ in the active materials, respectively [19]. According to the equivalent circuit, the impedance of a R_{sf} and R_{ct} of $LiNi_{1/3}Co_{1/3}Mn_{1/3}O_2@YF_3$ were calculated as 49.6 Ω and 71.1 Ω, which were smaller than those of pristine $LiNi_{1/3}Co_{1/3}Mn_{1/3}O_2$ (R_{sf}=83.8 Ω, R_{ct}=105.4 Ω). This result obviously indicated that the enhanced electrochemical performance was

attributed to the presence of YF_3–coating layer, which effectively suppressed the chemical instability ascribed to side-reactions between the electrode and electrolyte at high voltage.

Fig. 8 showed the cycling performance of the pristine and YF_3-coated $LiNi_{1/3}Co_{1/3}Mn_{1/3}O_2$ electrodes over 100 cycles, 5 C at 25°C and 1 C at 60°C , respectively. In comparison with the pristine $LiNi_{1/3}Co_{1/3}Mn_{1/3}O_2$, the capacity loss was greatly suppressed after coating with YF_3. As shown in Fig. 8(a), the initial discharge capacity at 5 C of $LiNi_{1/3}Co_{1/3}Mn_{1/3}O_2$ was 121 $mAh \cdot g^{-1}$ and found to decrease to 89 $mAh \cdot g^{-1}$ after 100 cycles (i.e., only 74% of its initial discharge capacity). The discharge capacity of the $LiNi_{1/3}Co_{1/3}Mn_{1/3}O_2@YF_3$ was found to decay gradually with continuous cycling, retaining 93% of its maximum discharge capacity after 100 cycles. When the cells were cycled at 1 C, the capacity retention increased from 53% for pristine $LiNi_{1/3}Co_{1/3}Mn_{1/3}O_2$ to 81% for $LiNi_{1/3}Co_{1/3}Mn_{1/3}O_2@YF_3$ (Fig. 8(b)). These results suggested that capacity fading was effectively suppressed by surface coating with YF_3. The side-reaction between the electrode and electrolyte should be responsible for the capacity fading for cathode material during extensive cycling especially at high operation temperature. For the coated samples, the YF_3 coating layer acted as a protective layer and prevented side-reactions between the electrode and electrolyte. This helped to improve the stability of electrode against HF attack and consequently enhance the cycling performance of the electrode.

The cyclic voltammetry profiles of the pristine and YF_3-coating samples in the first nine cycles at a scan of 0.1 mV s^{-1}, were shown in Figs. 9(a,b). A pair of distinct redox peaks was observed in the potential range of 3.6–4.0 V, which should be attributed to Ni^{2+}/Ni^{4+} alternating during the charging/discharging process. The

shifting of oxidation peak after the first cycle might be attributed to the electrode formation due to good electrical contact with the conductive agent, current collector and electrolyte [20,21]. In comparison with $LiNi_{1/3}Co_{1/3}Mn_{1/3}O_2$, the CV curves in the 2nd and 9th cycles of $LiNi_{1/3}Co_{1/3}Mn_{1/3}O_2@YF_3$ demonstrated a better overlapping degree, suggesting that $LiNi_{1/3}Co_{1/3}Mn_{1/3}O_2@YF_3$ possessed a better cyclic reversibility. The potential difference (Δ E) between anodic and cathodic peaks reflected the polarization degree of the electrode. The larger potential difference indicated the larger polarization [22]. Fig. 9(c) showed the cyclic voltammogram curves for $LiNi_{1/3}Co_{1/3}Mn_{1/3}O_2$ and $LiNi_{1/3}Co_{1/3}Mn_{1/3}O_2@YF_3$ after 100 cycles. The potential difference between oxidation and reduction of $LiNi_{1/3}Co_{1/3}Mn_{1/3}O_2@YF_3$ (0.181 V) was smaller than that of the $LiNi_{1/3}Co_{1/3}Mn_{1/3}O_2$ (0.237 V). The spinel phase with low conductivity was likely responsible for electrode polarization. The YF_3-coating was expected to effectively suppress the phase transformation of $LiNi_{1/3}Co_{1/3}Mn_{1/3}O_2$ particle from a layered to spinel structure. Similar results were reported by other groups [17,23]. The electrolyte decomposition on the surface of the active material at high operation voltage on cycling may also prevent direct interactions between electrode and electrolyte [16,24]. The CV measurements were consistent with the EIS measurements. The changes in voltage at the half point of the charge/discharge state during the charge/discharge process were shown in Fig. 9(d). The charge potential was observed to increase while the discharge potential decreased with increasing charge/discharge cycle. In comparison, the YF_3–coated sample exhibited a smaller change in potential than that of the pristine $LiNi_{1/3}Co_{1/3}Mn_{1/3}O_2$. This phenomenon would be attributed to the increase in electrode polarization due to side-reactions between the electrode and electrolyte. The obtained measurements were in good agreement with the CV measurements.

To investigate the impact of the YF_3–coating on the Li^+ diffusion kinetics of $LiNi_{1/3}Co_{1/3}Mn_{1/3}O_2$, the impedance spectra after 100 cycles under different charge/discharge states for $LiNi_{1/3}Co_{1/3}Mn_{1/3}O_2$ and $LiNi_{1/3}Co_{1/3}Mn_{1/3}O_2$@$YF_3$ electrodes were continuously measured during the lithium-ion insertion/extraction process. EIS plots (Z'' vs. Z') were shown in Fig. 10. According to the relationship between the real axis (Z') and the reciprocal square root($\omega^{-1/2}$) of the lower angular frequencies, the chemical diffusion coefficient of Li^+ (D_{Li}^+) can be calculated as follows[25]

$$Z' = \mathrm{R}_e + R_{ct} + \sigma_\omega \omega^{-1/2} \quad (1)$$

$$D_{Li}^+ = \left(\frac{2RT}{\sqrt{2} n^2 F^2 \sigma_w AC} \right)^2 = \frac{2R^2T^2}{n^4 F^4 \sigma_w^2 A^2 C^2} \quad (2)$$

where R, T and F were the mass gas constant, absolute temperature and Faraday's constant; A was the surface area of the electrode; n was the number of electrons per molecule during oxidation; C was the molar volume of active material; σ_w was the Warburg coefficient. Based on the linear plot slope of Z' *vs.* $\omega^{-1/2}$, the corresponding lithium diffusion coefficients at different charge/discharge states for $LiNi_{1/3}Co_{1/3}Mn_{1/3}O_2$ and $LiNi_{1/3}Co_{1/3}Mn_{1/3}O_2$@$YF_3$ electrodes could be calculated respectively (Fig. 11). Both electrodes exhibited similar Li^+ diffusion behavior and displayed a peak ranging from 3.8 to 4.2 V, which resulted from lithium-ion insertion into or extraction from the R-3m structure $LiMO_2$(M=Mn,Ni,Co) region. In comparison with $LiNi_{1/3}Co_{1/3}Mn_{1/3}O_2$, $LiNi_{1/3}Co_{1/3}Mn_{1/3}O_2$@$YF_3$ displayed larger Li^+ diffusion coefficients in the charge and discharge processes, indicating that YF_3–coating would readily facilitate Li^+ transferring at the interface of electrode/electrolyte. It was well-established that the electrochemical polarization of $LiNi_{1/3}Co_{1/3}Mn_{1/3}O_2$ electrode increased during the charge/discharge process due to

the formation of the resistive reaction layers and the dissolution of the cathode material in a liquid electrolyte [26]. The YF_3–coating layer would reduce the strain and defect generated by the Li^+ intercalation and extraction in the active material, mediating the increase in charge transfer resistance. This would, in turn, facilitate Li^+ transfer at the interface of the electrode/electrolyte and provide enhanced rate performance.

To elucidate the potential mechanism of the enhanced Li^+ diffusion kinetics of $LiNi_{1/3}Co_{1/3}Mn_{1/3}O_2$ by YF_3 coating, EIS measurements were carried out on $LiNi_{1/3}Co_{1/3}Mn_{1/3}O_2$ and $LiNi_{1/3}Co_{1/3}Mn_{1/3}O_2$@$YF_3$ cathode materials after 100 cycles at the full charge state from 0°C to -30°C (Figs. 12(a,b)). The EIS profiles were fit based on the equivalent circuit (shown in Fig.7(b)), and the fitted results revealed that $LiNi_{1/3}Co_{1/3}Mn_{1/3}O_2$ exhibited a more pronounced effect on charge-transfer resistance at the electrode-electrolyte interface as the operating temperature decreases. A higher R_{ct} generally indicated slower kinetics of the faradic reaction [27]. The activation energy (△G) of lithium-ion insertion/extraction within the pristine and the YF_3-coated $LiNi_{1/3}Co_{1/3}Mn_{1/3}O_2$ could be calculated by,

$$\log R_{ct} = \log A + \frac{\Delta G - R}{2.303RT} \tag{3}$$

where △G was the activation energy, T was the absolute temperature, R was the gas constant, and A was a temperature-independent constant. The temperature dependence of log Rct in the temperature range from 0°C to -30°C was shown in Fig. 12(c). The △G for $LiNi_{1/3}Co_{1/3}Mn_{1/3}O_2$ and $LiNi_{1/3}Co_{1/3}Mn_{1/3}O_2$@$YF_3$ were calculated as 69.69 $KJmol^{-1}$ and 49.77 $KJmol^{-1}$, respectively. Lower activation energy was indicative of faster Li-ion diffusion [28]. These results confirmed that YF_3 coating layer acted as a catalyst, accelerating the charge transfer process at the interface between the electrode

and electrolyte, which could well explain the enhanced Li^+ diffusion kinetics in Fig. 11.

High electrical conductivity is highly desirable for enhanced electrochemical performances of lithium ion battery. The forces of interaction with a crystal lattice have been shown to hinder electrons escaping from the material, creating a potential barrier on a material surface. Therefore, for removal of an electron from the material to occur, it should receive energy equal to the difference between the surface potential barrier and the Fermi level [29]. Surface potential maps of $LiNi_{1/3}Co_{1/3}Mn_{1/3}O_2$ and $LiNi_{1/3}Co_{1/3}Mn_{1/3}O_2@YF_3$ electrodes were obtained characterized using Kelvin probe atomic force microscopy. For comparison, the surface potential maps of Au foil as a reference sample were also measured (Fig. 13(b)). The surface potential maps of $LiNi_{1/3}Co_{1/3}Mn_{1/3}O_2$ and $LiNi_{1/3}Co_{1/3}Mn_{1/3}O_2@YF_3$ electrodes after 100 cycles showed that $LiNi_{1/3}Co_{1/3}Mn_{1/3}O_2@YF_3$ possessed a considerably smaller surface potential than that of $LiNi_{1/3}Co_{1/3}Mn_{1/3}O_2$ (Figs. 13(c,d)). These results suggested that the electrons required less energy to escape from the $LiNi_{1/3}Co_{1/3}Mn_{1/3}O_2@YF_3$ material, in turn enhancing the electrochemical performance.

It is worthy to note that surface potential difference (or electrostatic contact potential difference) between the tip and the sample originates from the difference in the work function of the electrically connected tip and the sample [30]. The surface potential ($\Delta\varphi$) is defined by:

$$\Delta\phi = \frac{\phi_{tip} - \phi_{sample}}{e} \tag{4}$$

where ϕ_{tip} and ϕ_{sample} are work functions of the tip and the sample, respectively, and e is the elementary charge. To evaluate the work function of surfaces, the work functions of the Pt/Ir-coated SFM-tip (ϕ_{tip}) was calibrated using Au foil as a

reference, whose work function (ϕ_{Au}) was considered constant (ϕ_{Au} =5.31eV). According to other researchers' work [31,32], the work functions of $LiNi_{1/3}Co_{1/3}Mn_{1/3}O_2$ and $LiNi_{1/3}Co_{1/3}Mn_{1/3}O_2@YF_3$ electrodes were calculated and shown in Fig. 14(a). The YF_3–coated sample was found to possess a smaller work function (~5.52 eV) than that (~6.08 eV) of the pristine one. A cathode with a Fermi level below the highest occupied molecular orbital (HOMO) has been previously shown to oxidize the electrolyte unless a passivation layer blocks electron transfer from the electrolyte HOMO to the cathode [2,33]. A schematic of the relative electron energies between cathode electrodes and the electrolyte was shown in Fig. 14(b). It can be deduced that the smaller work function would effectively reduce oxidation of the electrolyte and consequently improve thermodynamic stability of the cathode materials during the charge/discharge process.

The thermal stability of cathode materials is an important consideration in battery safety [34]. The thermal stability of the pristine and YF_3-coated $LiNi_{1/3}Co_{1/3}Mn_{1/3}O_2$ cathode was measured at the fully charged state of 4.5 V (vs. Li/Li+) using differential scanning calorimetry, as shown in Fig. 15. The first exothermic peak at 235 ^oC may be attributed to the decomposition of electrolyte on the cathode surface, while the second corresponds to electrolyte oxidation caused by oxygen released from $LiNi_{1/3}Co_{1/3}Mn_{1/3}O_2$ [35]. In the case of $LiNi_{1/3}Co_{1/3}Mn_{1/3}O_2$, the major exothermic peak was located at 237.8°C, with heat generation of 1.44 $mWmg^{-1}$. Meanwhile, an exothermic peak assigned to $LiNi_{1/3}Co_{1/3}Mn_{1/3}O_2@YF_3$ appeared at relatively high temperature of 253.7°C with relatively lower heat generation of 0.82 $mWmg^{-1}$. The higher exothermic peak temperature and lower heat generation indicate that the thermal stability of the electrode was improved by YF_3 coating. The enhanced thermal stability of $LiNi_{1/3}Co_{1/3}Mn_{1/3}O_2@YF_3$ cathode might

be attributed to the YF_3-coating layer, which possessed excellent thermal stability and effectively protects the active material from side reactions in the electrolyte [36].

4. Conclusions

$LiNi_{1/3}Co_{1/3}Mn_{1/3}O_2$ coated with YF_3 was prepared by a wet chemical process. In comparison with pristine $LiNi_{1/3}Co_{1/3}Mn_{1/3}O_2$, the YF_3–coated composite exhibits higher rate capability, better cyclability and better thermal stability. Analysis from electrochemical measurements showed that the improved electrochemical performances $LiNi_{1/3}Co_{1/3}Mn_{1/3}O_2$@$YF_3$ might be attributed to smaller charge-transfer resistances, higher lithium diffusion rates, and the stable electrolyte/electrode interfacial structure. To some extent, the possible mechanism discussed in this study would help to clarify the enhanced performances of cathode materials with surface modification in terms of interfacial effect.

Acknowledgements

This work is supported by a grant from Key Project of Department of Science & Technology of Fujian Province (No.2014H0020), Program for New Century Excellent Talents in University of Fujian Province (No.JA14069) and Project A of Education Bureau of Fujian Province (No.JA12067).

References

[1] M. Armand, J.-M. Tarascon, Building better batteries, Nature 451 (2008) 652-657.

[2] J. B. Goodenough, K. -S. Park, The Li-Ion Rechargeable Battery: A Perspective, J. Am. Chem. Soc. 135 (2013) 1167–1176.

[3] S. Goriparti, E. Miele, F. D. Angelis, E. D. Fabrizio, R. P. Zaccaria, C. Capiglia, Review on recent progress of nanostructured anode materials for Li-ion batteries, J. Power Sources 257 (2014) 421-443.

[4] N. Alias, A. A. Mohamad, Advances of aqueous rechargeable lithium-ion battery: A review, J. Power Sources 274 (2015) 237–251.

[5] A. Fotouhi, D. J. Auger, K. Propp, S. Longo, M. Wild, A review on electric vehicle battery modelling: From Lithium-ion toward Lithium–Sulphur, Renew. Sust. Energ. Rev. 56 (2016) 1008–1021.

[6] M. Hu, X. Pang, Z. Zhou, Recent progress in high-voltage lithium ion batteries, J. Power Sources 237 (2013) 229-242.

[7] P. B. Samarasingh, A. Wijayasinghe , M. Behm, L. Dissanayake, G. Lindbergh, Development of cathode materials for lithium ion rechargeable batteries based on the system $Li(Ni_{1/3}Mn_{1/3}Co_{(1/3-x)}M_x)O2$, (M = Mg, Fe, Al and x =0.00 to 0.33), Solid State Ionics 268 (2014) 226-230.

[8] K. Yang, L.Z. Fan, J. Guo, X. H. Qu, Significant improvement of electrochemical properties of AlF_3-coated $LiNi_{0.5}Co_{0.2}Mn_{0.3}O_2$ cathode materials, Electrochim. Acta 63 (2012) 363–368.

[9] B. Xu, D. N. Qian, Z. Y. Wang, Y. S. Meng, Recent progress in cathode materials research for advanced lithium ion batteries, Mater. Sci. Eng. R 73 (2012) 51–65.

[10] S. Uchida, N. Zettsu, K. Hirata, K. Kami, K. Teshima, High-voltage capabilities of ultra-thin Nb_2O_5 nanosheet coated $LiNi_{1/3}Mn_{1/3}Co_{1/3}O_2$ cathodes, RSC adv. 6 (2016) 67514-67519.

[11] Y. Xie, D.Gao, L. L.Zhang, J. J. Chen, S. Cheng, H. F. Xiang, CeF_3-modified $LiNi_{1/3}Mn_{1/3}Co_{1/3}O_2$ cathode material for high-voltage Li-ion batteries, Ceram. Int. 142 (2016) 14587-14594.

[12] A. Yano, A. Ueda, M. Shikano, H. Sakaebe, Z. Ogumi, Surface structure and high-voltage charging/discharging performance of low-content Zr-oxide-coated $LiNi_{1/3}Co_{1/3}Mn_{1/3}O_2$, J. Electrochem. Soc. 163 (2016) A75-A82.

[13] Q. B. Zhang, L. Wang, C. H. Zhu, Z. P. Sun, D. D. Lv, W. Ren, L. Bian, J. B. Xu, A. M. Chang, Enhanced electrochemical capability of $LiNi_{1/3}Co_{1/3}Mn_{1/3}O_2$ cathode materials coated with fluoroborate glass for lithium-ion batteries, Chem. Electro. Chem. (2017) doi:10.1002/celc.201600828.

[14] V. Trnovcova, L. S. Garashina, A. Skubla, P. P. Fedorov, R. Cicka, E. A. Krivandina, B. P. Sobolev, Structural aspects of fast ionic conductivity of rare earth fluorides, Solid State Ionics 157 (2003) 195-201.

[15] B. L. Liu, Z. H. Zhang, J. K. Wan, S. F. Liu, Improved electrochemical properties of YF_3-coated $Li_{1.2}Mn_{0.54}Ni_{0.13}Co_{0.13}O_2$ as cathode for Li-ion batteries, Ionics (2017) doi:10.1007/s11581-016-1950-4.

[16] W. B. Zhu, Z. Y. Zhuang, Z. Y. Lin, Y. M. Yang, Y. B. Lin, Z. G. Huang, Enhanced electrochemical properties and thermal stability of $LiNi_{1/3}Co_{1/3}Mn_{1/3}O_2$ by surface modification with Eu_2O_3, Ionics 22 (2016) 1533-1540.

[17] L. N. Cong, Q. Zhao, Z. Wang, Y. H. Zhang, X. L. Wu, J. P. Zhang, R. S. Wang, H. M. Xie, L. Q. Sun, $(PO_4)^{3-}$ polyanions doped $LiNi_{1/3}Co_{1/3}Mn_{1/3}O_2$:

An ultrafast-rate, long-life and high-voltage cathode material for Li-ion rechargeable batteries, Electrochim. Acta 201 (2016) 8-19.

[18] X. Guo, L. N. Cong, Q. Zhao, L. H. Tai, X. L. Wu, J. P. Zhang, R. S. Wang, H. M. Xie, L. Q. Sun, Enhancement of electrochemical performance of $LiNi_{1/3}Co_{1/3}Mn_{1/3}O_2$ by surface modification with MnO_2, J. Alloys Compd. 651 (2015) 12-18.

[19] X. Li, H. Peng, M. S. Wang, X. Zhao, P. X. Huang, W. Yang, J. Xu, Z. Q. Wang, M. Z. Qu, Z. L. Yu, Enhanced electrochemical performance of Zr-modified layered $LiNi_{1/3}Co_{1/3}Mn_{1/3}O_2$ cathode material for lithium ion batteries, ChemElectroChem 3 (2016) 130-137.

[20] F. Wu, M. Wang, Y. F. Su, S. Chen, B. Xu, Effect of TiO_2-coating on the electrochemical performances of $LiCo_{1/3}Ni_{1/3}Mn_{1/3}O_2$, J. Power Sources 191 (2009) 628-632.

[21] P. R. Ilango, T. Subburaj, K. Prasanna, Y. N. Jo, C. W. Lee, Physical and electrochemical performance of $LiNi_{1/3}Co_{1/3}Mn_{1/3}O_2$ cathodes coated by Sb_2O_3 using a sol–gel process, Mater. Chem. Phys. 158 (2015) 45-51.

[22] J. T. Son, E. J. Cairns, Characterization of $LiCoO_2$ coated $Li_{1.05}Ni_{0.35}Co_{0.25}Mn_{0.4}O_2$ cathode material for lithium secondary cells, J. Power Sources 166 (2007) 343-347.

[23] P. K. Nayak, J. Grinblat, M. Levi, Y. Wu, B. Powell, D. Aurbach, TEM and Raman spectroscopy evidence of layered to spinel phase transformation in layered $LiNi_{1/3}Mn_{1/3}Co_{1/3}O_2$ upon cycling to higher voltages, J. Electroanal. Chem. 733 (2014) 6-19.

[24]F. Wu, M. Wang, Y. F. Su, S. Chen, Surface modification of $LiCo_{1/3}Ni_{1/3}Mn_{1/3}O_2$ with Y_2O_3 for lithium-ion battery, J. Power Sources 189 (2009) 743-747.

[25]Z. Y. Lin, W. B. Zhu, Z. S. Wang, Y. M. Yang, Y. B. Lin, Z. G. Huang, Synthesis of carbon-coated $Li_4Ti_5O_{12}$ nanosheets as anode materials for high-performance lithium-ion batteries, J. Alloys Compd. 687 (2016) 232-239.

[26]X. Li, W. He, L. Chen, W. Guo, J. Chen, Z. Xiao, Hydrothermal synthesis and electrochemical performance studies of Al_2O_3-coated $LiNi_{1/3}Co_{1/3}Mn_{1/3}O_2$ for lithium-ion batteries, Ionics 20 (2013) 833-840.

[27]Y. B. Lin, Y. Lin, T. Zhou, G. Y. Zhao, Y. D. Huang, Z. G. Huang, Enhanced electrochemical performances of $LiFePO_4$/C by surface modification with Sn nanoparticles, J. Power Sources 226 (2013) 20-26.

[28]M. Okubo, Y. Tanaka, H. S. Zhou, I.Honma, Determination of activation energy for Li ion diffusion in electrodes, J. Phys. Chem. B 113 (2009) 2840-2847.

[29]B. Bhushan, Scanning Probe Microscopy in Nanoscience and Nanotechnology, Springer Heidelberg Dordrecht London New York.

[30]A.L. Zharin, D.A. Rigney, Application of the contact potential difference technique for on-line rubbing surface monitoring, Tribol. Lett. 4 (1998) 205-213.

[31]S. C. Nagpurea, B. Bhushana, S. S. Babub, urface potential measurement of aged Li-ion batteries using Kelvin probe microscopy, J. Power Sources 196 (2011) 1508-1512.

[32] A. Sharma, M. Untch, J. S. Quinton, R. Berger, G. Andersson, D. A. Lewis, Nanoscale heterogeniety and workfunction variations in ZnO thin films, Appl. Surf. Sci. 363 (2016) 516-521.

[33] J. B. Goodenough, Y. Kim, Challenges for rechargeable Li batteries, Chem. Mater. 22 (2010) 587-603.

[34] W. Chang, J. W. Choi, J.-Ch. Im, J. K. Lee, Effects of ZnO coating on electrochemical performance and thermal stability of $LiCoO_2$ as cathode material for lithium-ion batteries, J. Power Sources 195 (2010) 320-326.

[35] Y. Baba, S. Okada, J. Yamaki, Thermal stability of Li_xCoO_2 cathode for lithium ion battery, Solid State Ionics 148 (2002) 311-316.

[36] Q. Fu, F. Du, X. Bian, Y. Wang, X. Yan, Y. Zhang, K. Zhu, G.C. Chen, Y. W. Wei, Electrochemical performance and thermal stability of $Li_{1.18}Co_{0.15}Ni_{0.15}Mn_{0.52}O_2$ surface coated with the ionic conductor Li_3VO_4, J. Mater. Chem. A 2 (2014) 7555-7562.

Figure Captions

Fig. 1 Schematic illustration of the preparation process for $LiNi_{1/3}Co_{1/3}Mn_{1/3}O_2@YF_3$ powders.

Fig. 2 XRD patterns of $LiNi_{1/3}Co_{1/3}Mn_{1/3}O_2$, $LiNi_{1/3}Co_{1/3}Mn_{1/3}O_2@YF_3$ and YF_3 powders.

Fig. 3 SEM images of (a,b) $LiNi_{1/3}Co_{1/3}Mn_{1/3}$ and (c,d) $LiNi_{1/3}Co_{1/3}Mn_{1/3}O_2@YF_3$ Powders.

Fig. 4 Element maps of $LiNi_{1/3}Co_{1/3}Mn_{1/3}O_2@YF_3$ particles.

Fig. 5 (a) HR-TEM images and (b) EDS of $LiNi_{1/3}Co_{1/3}Mn_{1/3}O_2@YF_3$ powder.

Fig. 6 (a) Rate capability of the pristine and $LiNi_{1/3}Co_{1/3}Mn_{1/3}O_2@YF_3$ electrodes at 25 ^oC; (b,c) Discharge curves of the pristine and YF_3-coated $LiNi_{1/3}Co_{1/3}Mn_{1/3}O_2$ electrodes at various discharge rate in the range 3.0-4.5V.

Fig. 7 (a) EIS profiles of $LiNi_{1/3}Co_{1/3}Mn_{1/3}O_2$ and $LiNi_{1/3}Co_{1/3}Mn_{1/3}O_2@YF_3$ at full charged state after rate test; (b) The equivalent circuit for EIS fitting.

Fig. 8 Cycling performances of the pristine and $LiNi_{1/3}Co_{1/3}Mn_{1/3}O_2@YF_3$ (a) at 5C and 25^oC; (b) at 1C and 60 ^oC.

Fig. 9 Cyclic voltammogram curves of (a) $LiNi_{1/3}Co_{1/3}Mn_{1/3}O_2$ and (b) $LiNi_{1/3}Co_{1/3}Mn_{1/3}O_2@YF_3$ electrodes in the first 9 cycles at $0.1mVs^{-1}$; (c) Cyclic voltammogram curves for the pristine and YF_3-coated $LiNi_{1/3}Co_{1/3}Mn_{1/3}O_2$ samples after 100 cycles; (d) Changes of voltage at half charge/discharge capacity with different cycles at 1C for both electrodes.

Fig. 10 The impedance spectra of $LiNi_{1/3}Co_{1/3}Mn_{1/3}O_2$ and $LiNi_{1/3}Co_{1/3}Mn_{1/3}O_2@YF_3$ electrodes after 100 cycles under different charge/discharge states.

Fig. 11 Lithium ion diffusion coefficients at different charge/discharge states for

.

Figure 1

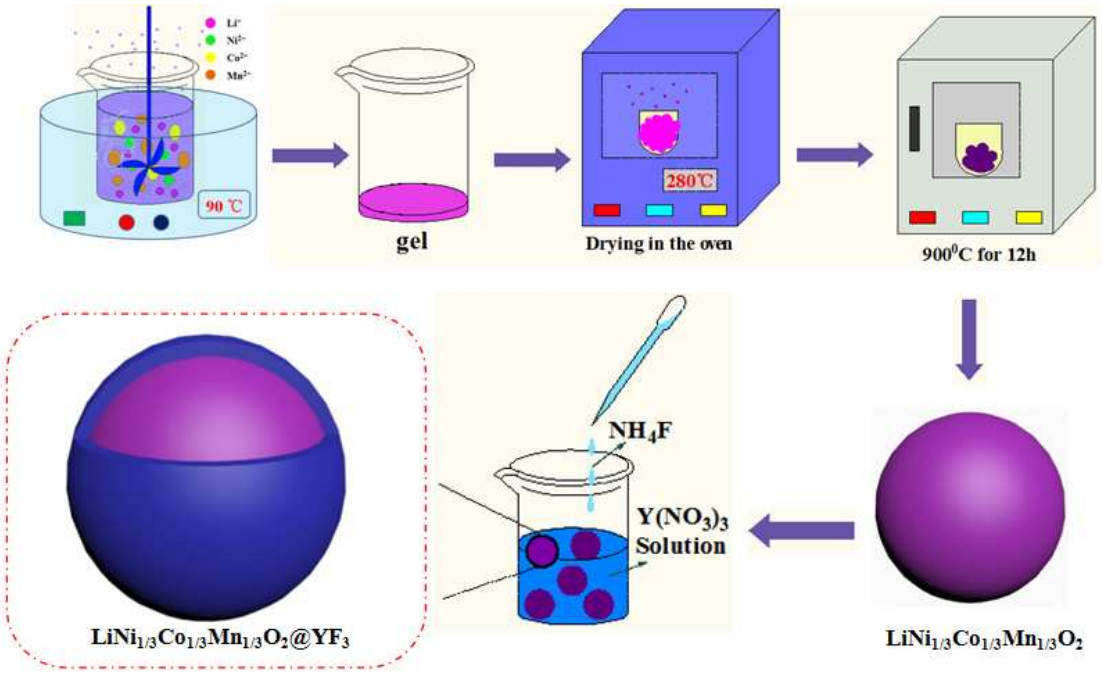

Figure 2

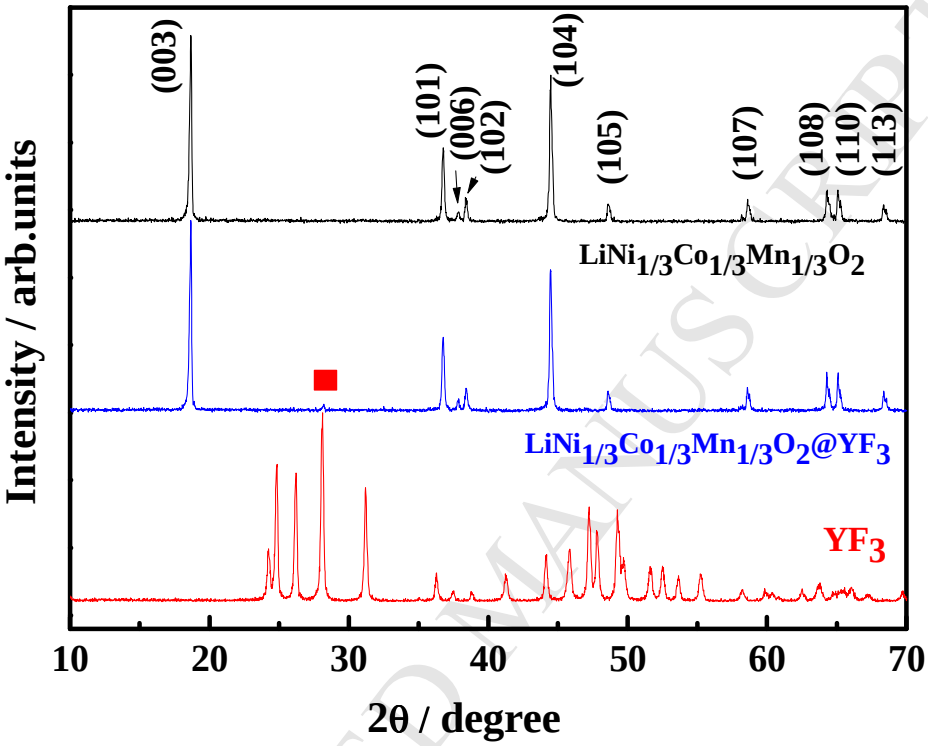

Figure 3

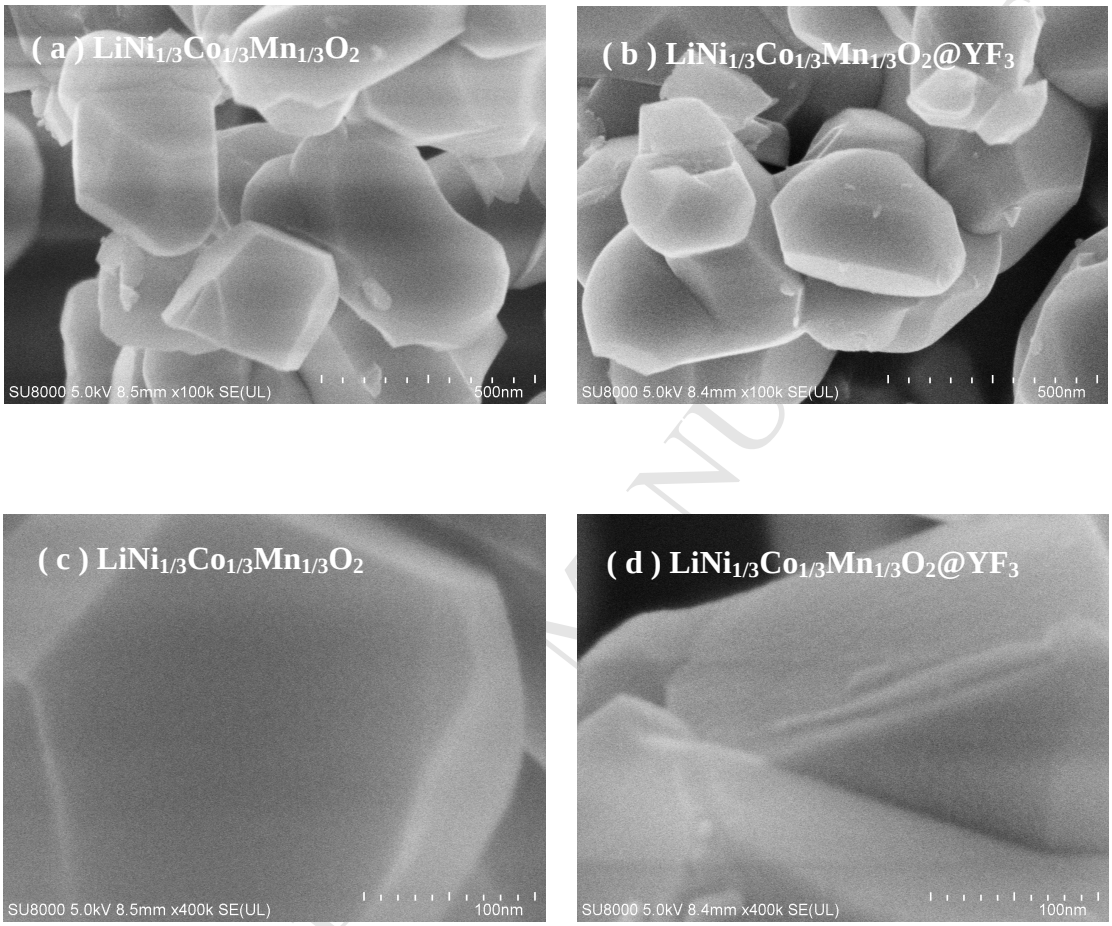
(a) LiNi1/3Co1/3Mn1/3O2
SU8000 5.0kV 8.5mm x100k SE(UL)
500nm
(b) LiNi1/3Co1/3Mn1/3O2@YF3
SU8000 5.0kV 8.4mm x100k SE(UL)
500nm
(c) LiNi1/3Co1/3Mn1/3O2
SU8000 5.0kV 8.5mm x400k SE(UL)
100nm
(d) LiNi1/3Co1/3Mn1/3O2@YF3
SU8000 5.0kV 8.4mm x400k SE(UL)
100nm

Figure 4

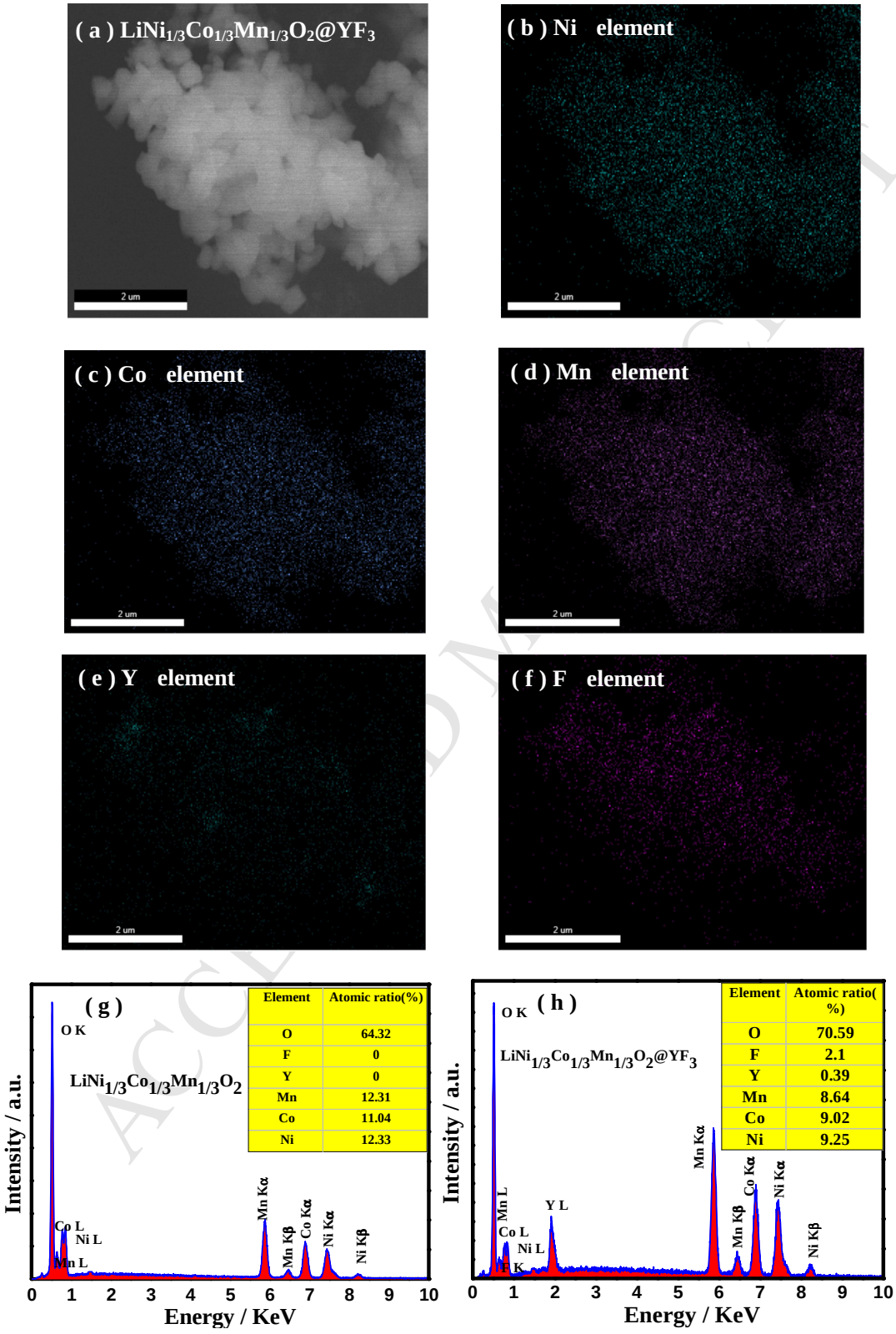
(a) LiNi1/3Co1/3Mn1/3O2@YF3
(b) Ni element
(c) Co element
(d) Mn element
(e) Y element
(f) F element
2 um
(g)
O K
LiNi1/3Co1/3Mn1/3O2
Element
Atomic ratio(%)
O 64.32
F 0
Y 0
Mn 12.31
Co 11.04
Ni 12.33
Co L
Ni L
Mn L
Mn Kα
Mn Kβ
Co Kα
Ni Kα
Ni Kβ
Intensity / a.u.
Energy / KeV
(h)
O K
LiNi1/3Co1/3Mn1/3O2@YF3
Element
Atomic ratio(%)
O 70.59
F 2.1
Y 0.39
Mn 8.64
Co 9.02
Ni 9.25
Mn L
Co L
Ni L
F K
Y L
Mn Kα
Mn Kβ
Co Kα
Ni Kα
Ni Kβ
Intensity / a.u.
Energy / KeV

Figure 5

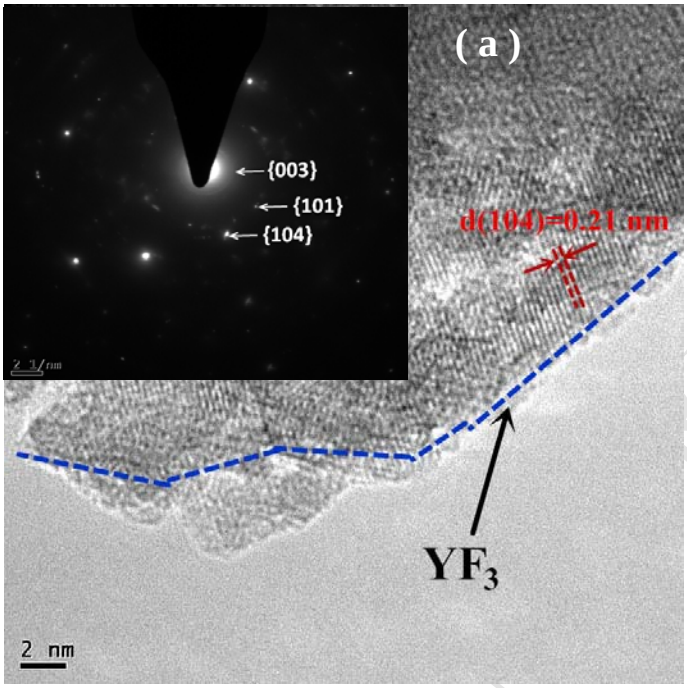
(a)
{003}
{101}
{104}
d(104)=0.21 nm
YF3
2 nm

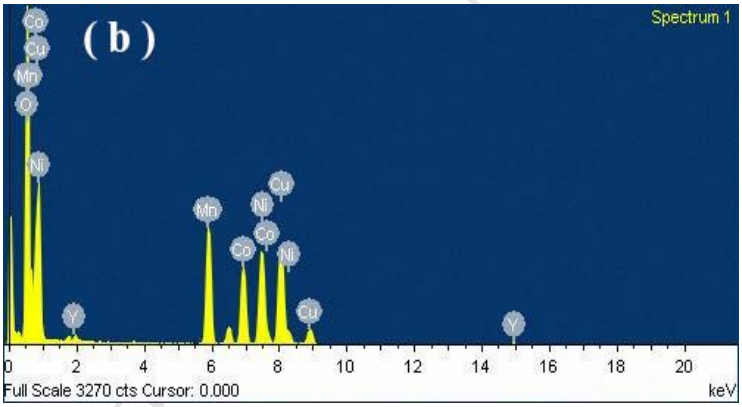
(b)
Spectrum 1
Co
Cu
Mn
O
Ni
Y
0
2
4
6
8
10
12
14
16
18
20
Full Scale 3270 cts Cursor: 0.000
keV

Figure 6

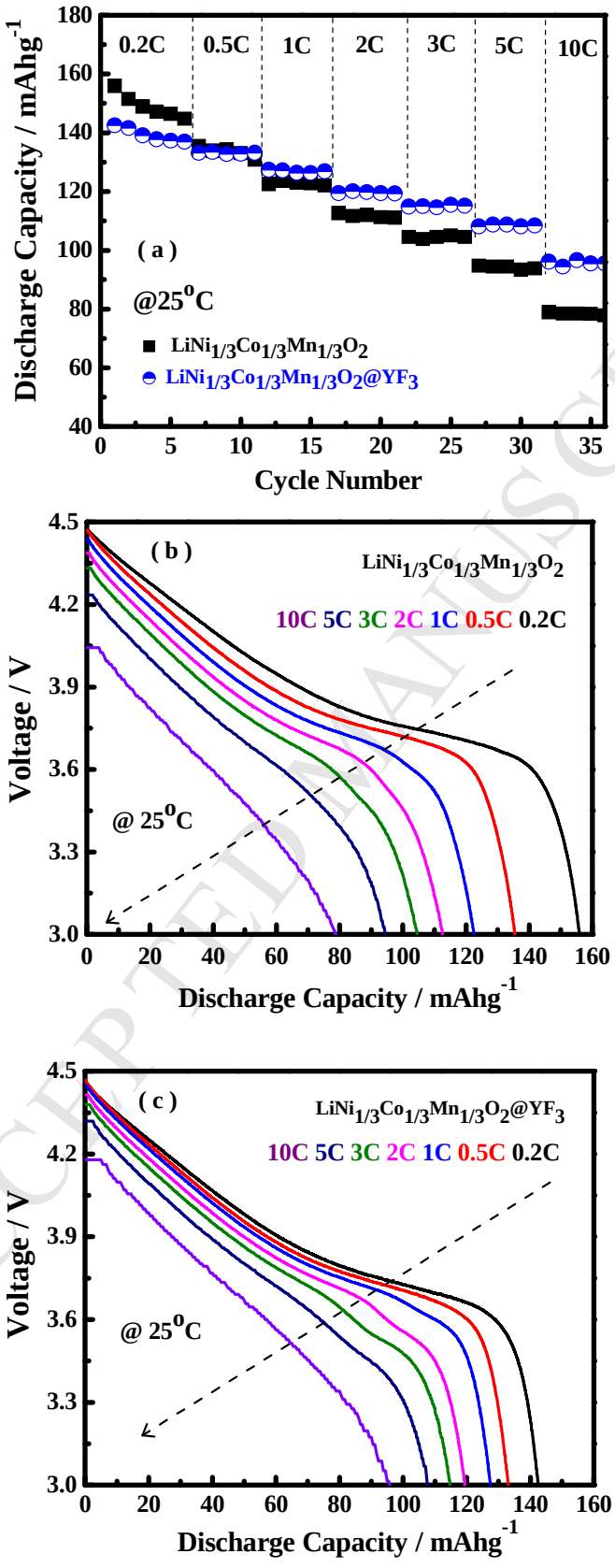
0.2C
0.5C
1C
2C
3C
5C
10C
(a)
@25°C
LiNi1/3Co1/3Mn1/3O2
LiNi1/3Co1/3Mn1/3O2@YF3
Discharge Capacity / mAhg-1
Cycle Number
(b)
LiNi1/3Co1/3Mn1/3O2
10C 5C 3C 2C 1C 0.5C 0.2C
@ 25°C
Voltage / V
Discharge Capacity / mAhg-1
(c)
LiNi1/3Co1/3Mn1/3O2@YF3
10C 5C 3C 2C 1C 0.5C 0.2C
@ 25°C
Voltage / V
Discharge Capacity / mAhg-1

Figure 7

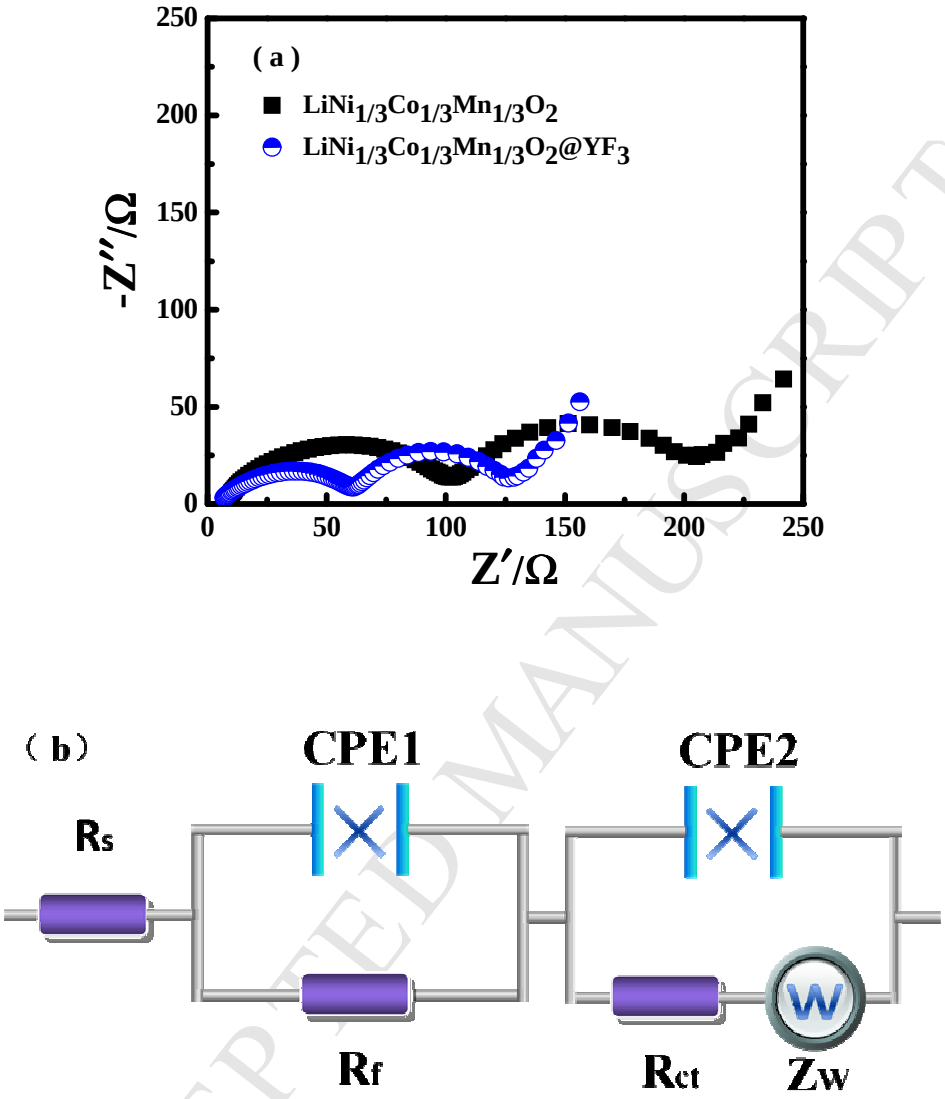

Figure 8

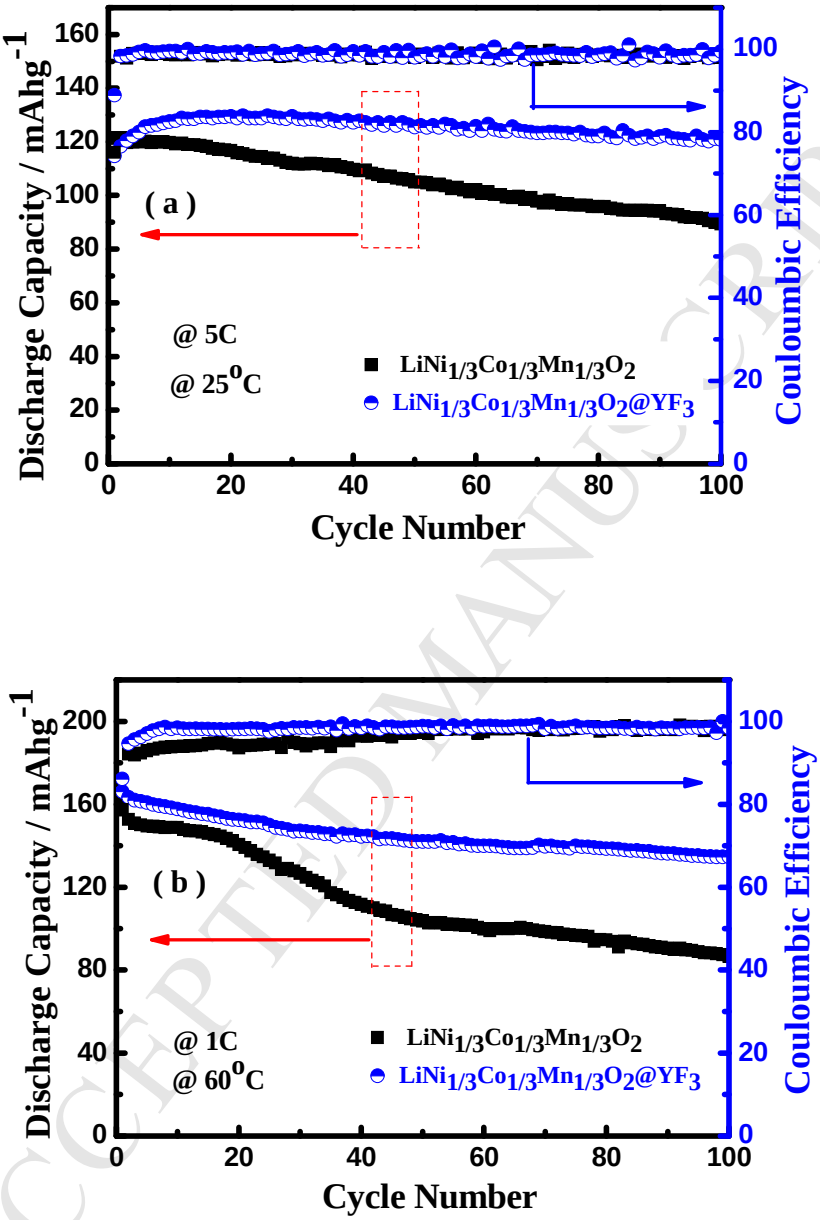

Figure 9

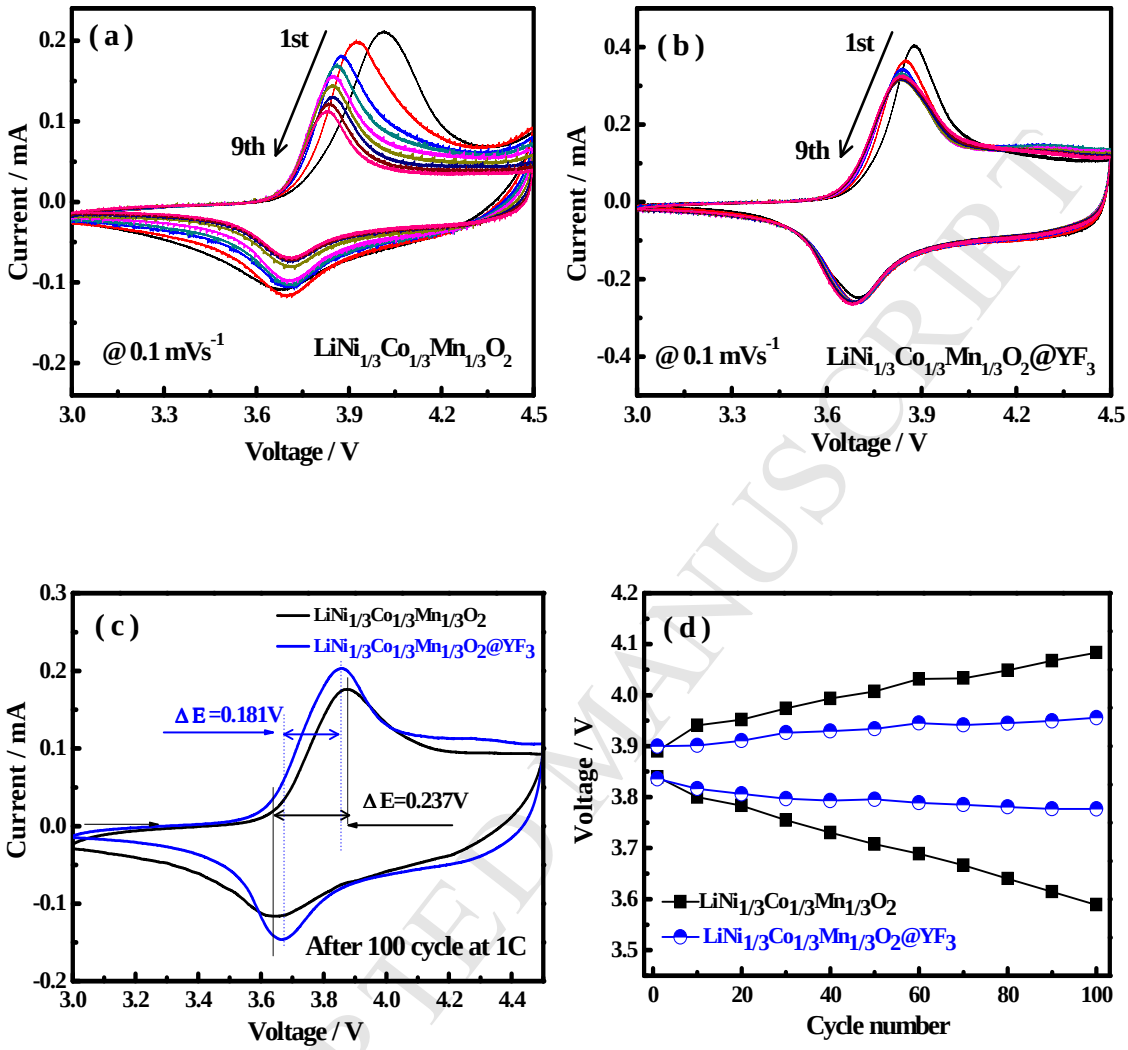

Figure 10

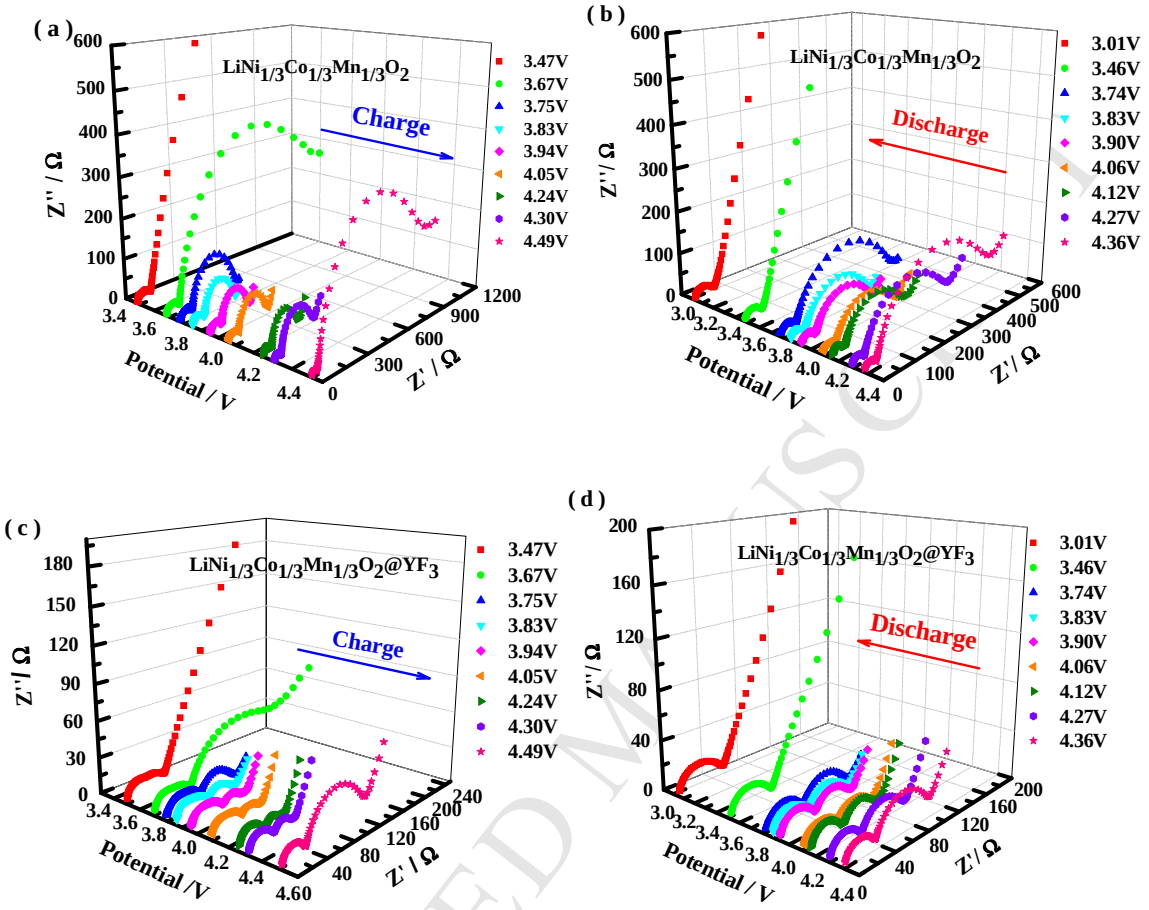
(a)
LiNi1/3Co1/3Mn1/3O2
Charge
Z'' / Ω
Potential / V
Z` / Ω
3.47V
3.67V
3.75V
3.83V
3.94V
4.05V
4.24V
4.30V
4.49V
(b)
LiNi1/3Co1/3Mn1/3O2
Discharge
Z'' / Ω
Potential / V
Z' / Ω
3.01V
3.46V
3.74V
3.83V
3.90V
4.06V
4.12V
4.27V
4.36V
(c)
LiNi1/3Co1/3Mn1/3O2@YF3
Charge
Z'' / Ω
Potential /V
Z` / Ω
3.47V
3.67V
3.75V
3.83V
3.94V
4.05V
4.24V
4.30V
4.49V
(d)
LiNi1/3Co1/3Mn1/3O2@YF3
Discharge
Z'' / Ω
Potential / V
Z' / Ω
3.01V
3.46V
3.74V
3.83V
3.90V
4.06V
4.12V
4.27V
4.36V

Figure 11

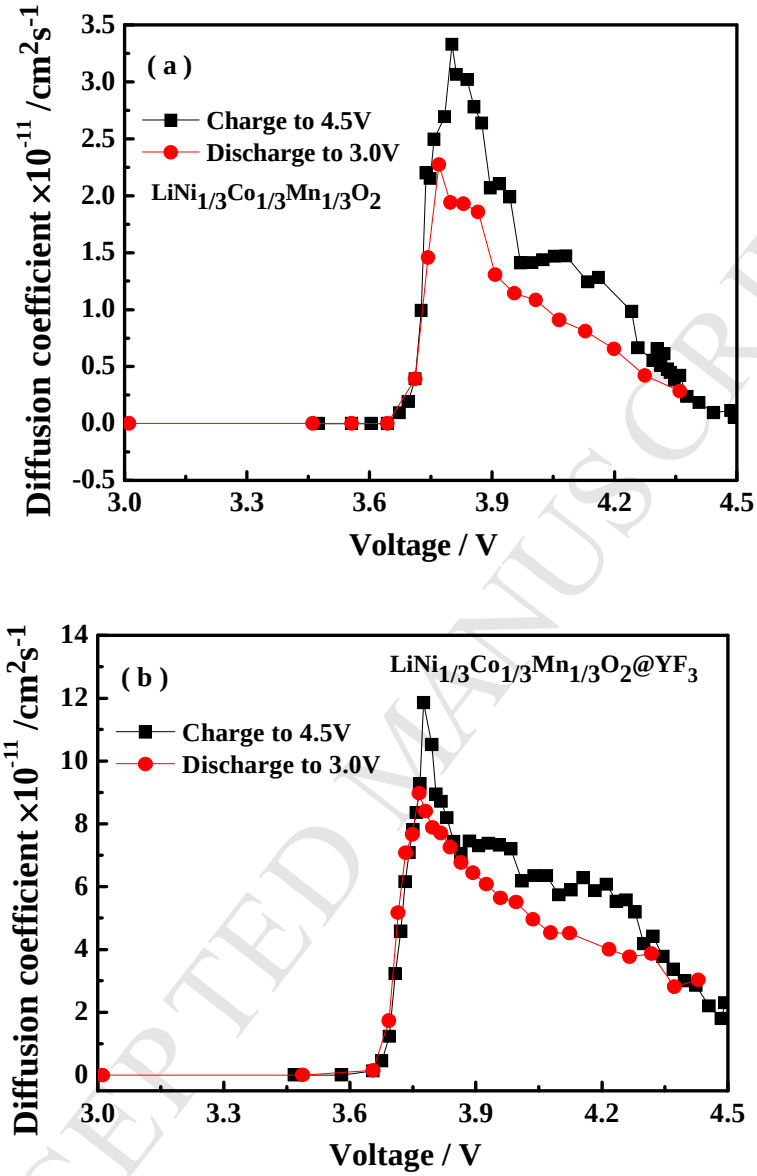

Figure 12

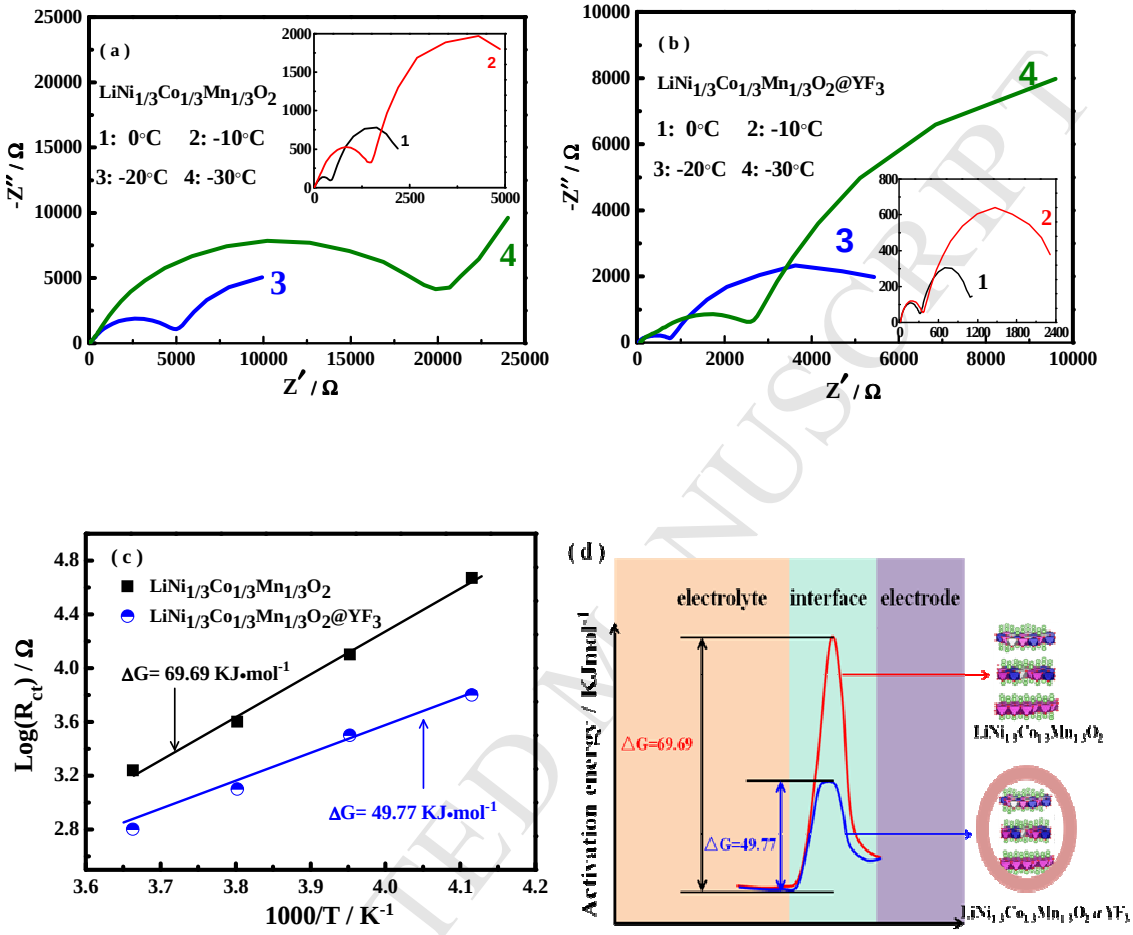
(a)
LiNi1/3Co1/3Mn1/3O2
1: 0°C 2: -10°C
3: -20°C 4: -30°C
-Z'' / Ω
Z' / Ω
(b)
LiNi1/3Co1/3Mn1/3O2@YF3
1: 0°C 2: -10°C
3: -20°C 4: -30°C
-Z'' / Ω
Z' / Ω
(c)
LiNi1/3Co1/3Mn1/3O2
LiNi1/3Co1/3Mn1/3O2@YF3
ΔG= 69.69 KJ•mol-1
ΔG= 49.77 KJ•mol-1
Log(Rct) / Ω
1000/T / K-1
(d)
electrolyte
interface
electrode
Activation energy / KJmol-1
△G=69.69
△G=49.77
LiNi1/3Co1/3Mn1/3O2
LiNi1/3Co1/3Mn1/3O2@YF3

Figure 13

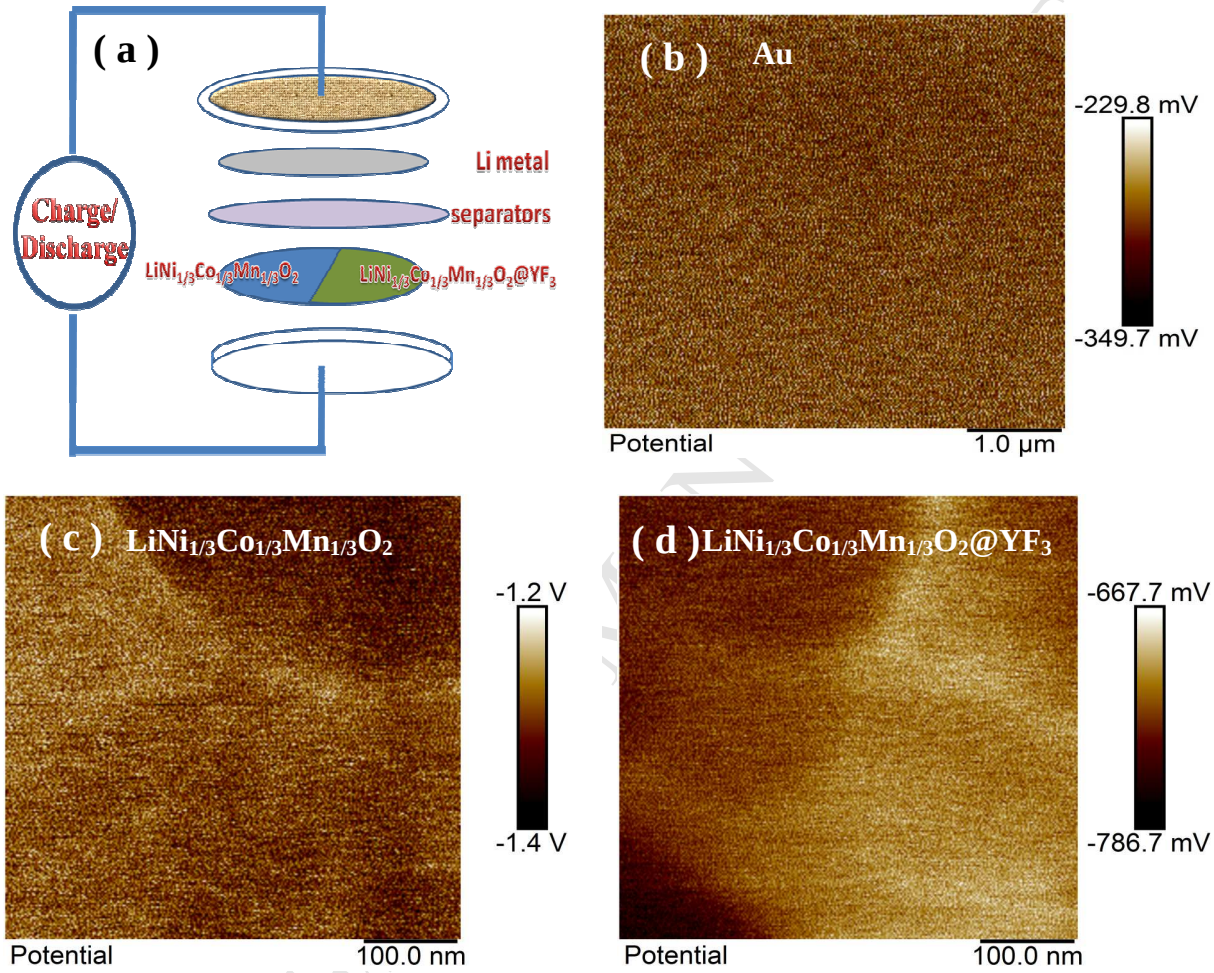
(a)
Charge/
Discharge
Li metal
separators
LiNi1/3Co1/3Mn1/3O2
LiNi1/3Co1/3Mn1/3O2@YF3
(b) Au
-229.8 mV
-349.7 mV
Potential
1.0 μm
(c) LiNi1/3Co1/3Mn1/3O2
-1.2 V
-1.4 V
Potential
100.0 nm
(d)LiNi1/3Co1/3Mn1/3O2@YF3
-667.7 mV
-786.7 mV
Potential
100.0 nm

Figure 14

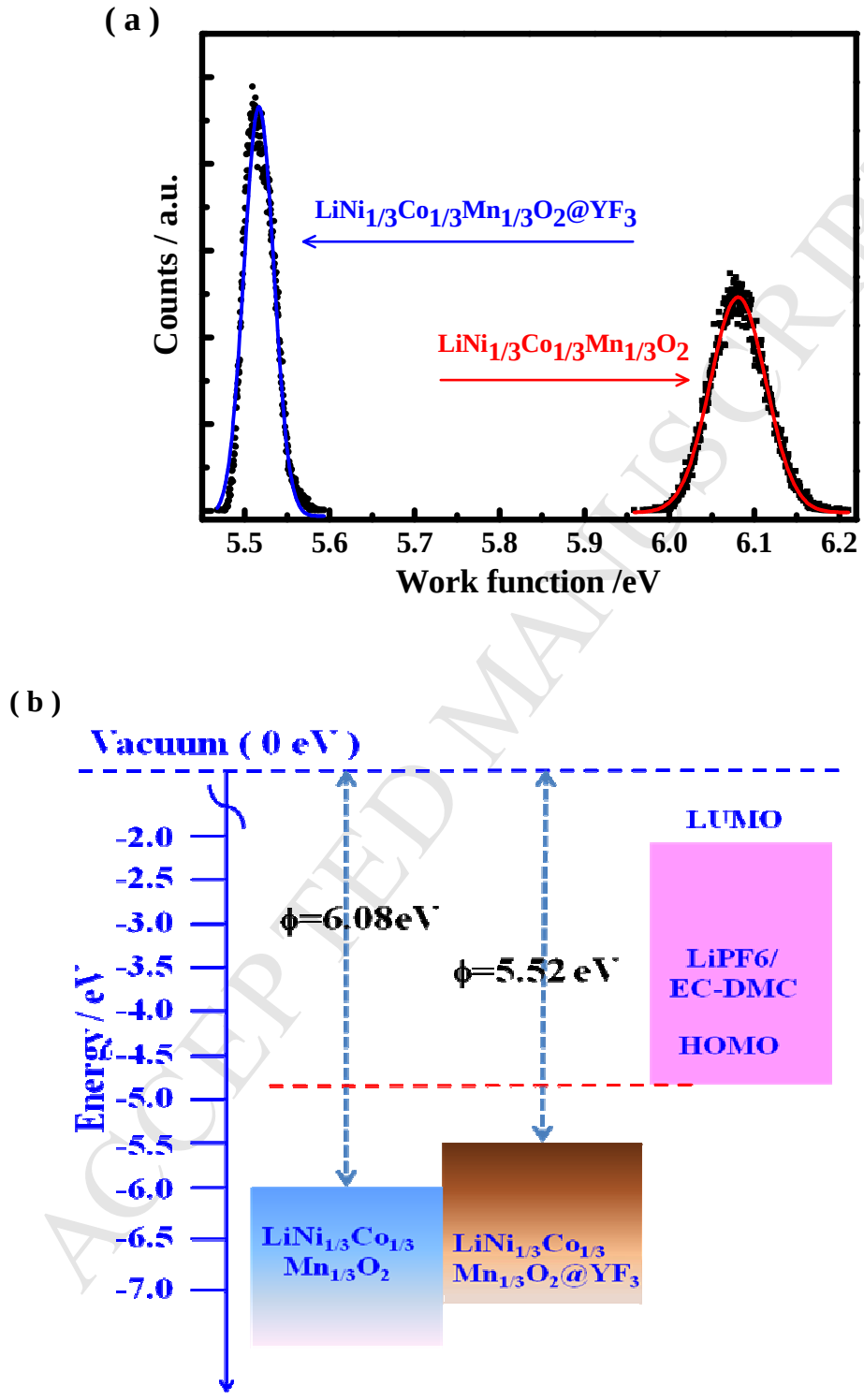

Figure 15

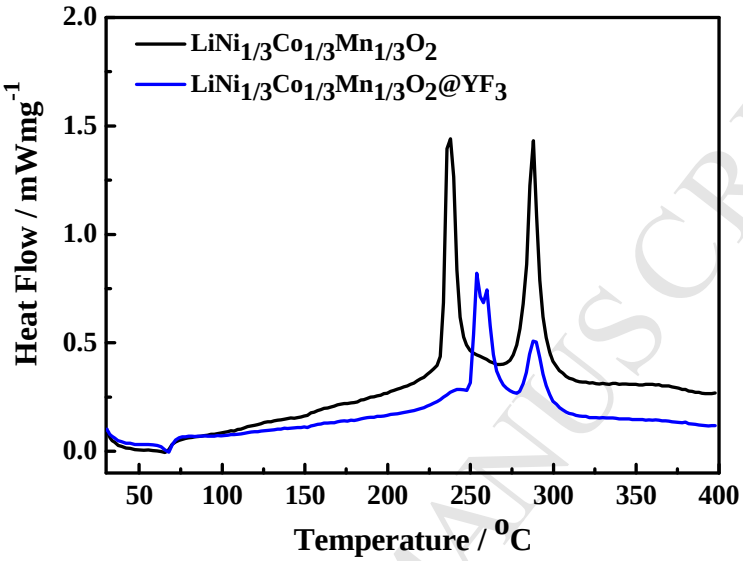

Research highlights

- YF_3–coating improves the rate performances and cyclability of $LiNi_{1/3}Co_{1/3}Mn_{1/3}O_2$.
- YF_3–coating reduces charge-transfer resistance and enhances Li^+ diffusion kinetics.
- YF_3–coating reduces work function of composite and enhances the thermal stability.